The Astrophysical Journal, 933:107 (10pp), 2022 July 1 https://doi.org/10.3847/1538-4357/ac7320

Formation of the Simplest Amide in Molecular Clouds: Formamide (NH_2CHO) and Its Derivatives in H_2O-rich and CO-rich Interstellar Ice Analogs upon VUV Irradiation

K.-J. Chuang[1,3], C. Jäger[1], S. A. Krasnokutski[1], D. Fulvio[2,4], and Th. Henning[2]
[1] Laboratory Astrophysics Group of the Max Planck Institute for Astronomy at the Friedrich Schiller University Jena, Institute of Solid State Physics, Helmholtzweg 3, D-07743 Jena, Germany; chuang@strw.leidenuniv.nl
[2] Max Planck Institute for Astronomy, Königstuhl 17, D-69117 Heidelberg, Germany
Received 2021 September 21; revised 2022 May 20; accepted 2022 May 23; published 2022 July 7

Abstract

The astronomical detection of formamide (NH_2CHO) toward various star-forming regions and in cometary material implies that the simplest amide might have an early origin in dark molecular clouds at low temperatures. Laboratory studies have proven the efficient NH_2CHO formation in interstellar CO:NH_3 ice analogs upon energetic processing. However, it is still under debate, whether the proposed radical–radical recombination reactions forming complex organic molecules remain valid in an abundant H_2O environment. The aim of this work was to investigate the formation of NH_2CHO in H_2O- and CO-rich ices under conditions prevailing in molecular clouds. Therefore, different ice mixtures composed of H_2O:CO:NH_3 (10:5:1), CO:NH_3 (4:1), and CO:NH_3 (0.6:1) were exposed to vacuum ultraviolet photons in an ultra-high vacuum chamber at 10 K. Fourier-transform infrared spectroscopy was utilized to monitor in situ the initial and newly formed species as a function of photon fluence. The infrared spectral identifications are complementarily secured by a temperature-programmed desorption experiment combined with a quadrupole mass spectrometer. The energetic processing of CO:NH_3 ice mixtures mainly leads to the formation of NH_2CHO, along with its chemical derivatives such as isocyanic acid (HNCO) and cyanate ion (OCN^-). The formation kinetics of NH_2CHO shows an explicit dependency on ice ratios and compositions; the highest yield is found in H_2O-rich ice. The astronomical relevance of the resulting reaction network is discussed.

Unified Astronomy Thesaurus concepts: Astrochemistry (75); Laboratory astrophysics (2004); Dense interstellar clouds (371); Surface processes (2116)

1. Introduction

Complex organic molecules (COMs) have been widely observed in massive molecular clouds, high- and low-mass protostars, and cometary material (see reviews by Herbst & van Dishoeck 2009; Herbst 2017; Altwegg et al. 2019). Among the successfully identified O-, N-, and S-bearing COMs, some of them attract exceptional attention in the field of astrochemistry due to their potential role in the extraterrestrial origin of building blocks of life (Muñoz Caro et al. 2002; Meierhenrich 2005; Nuevo et al. 2008; Fulvio et al. 2021; Ioppolo et al. 2021). For example, formamide (NH_2CHO) has been suggested to be an important precursor for the formation of nucleobases (e.g., adenine, uracil, thymine, cytosine, and guanine), which are found in RNA and/or DNA structures (Saladino et al. 2006; Barks et al. 2010; Rotelli et al. 2016).

In astronomical observations, NH_2CHO was first detected by Rubin et al. (1971) toward Sgr B2. Later, it has been observed by follow-up searches in various high-mass protostellar objects (Bisschop et al. 2007; Halfen et al. 2011; Isokoski et al. 2013; Jones et al. 2013; Neill et al. 2014; Suzuki et al. 2018; Colzi et al. 2021). NH_2CHO has also been identified toward several solar-mass stars and shock regions (Takahiro et al. 2012; Kahane et al. 2013; Mendoza et al. 2014; López-Sepulcre et al. 2015; Taquet et al. 2015; Coutens et al. 2016; Imai et al. 2016; Lee et al. 2017; Oya et al. 2017; Marcelino et al. 2018). A detailed list of astronomical observations can be found in the review by López-Sepulcre et al. (2019). Although the detection of NH_2CHO in prestellar cores is still lacking, the common detection of the simplest amide in cometary comae, which have been considered to represent the pristine interstellar ice composition, suggests that it could have an early and cold origin from dense molecular clouds (Bockelee-Morvan et al. 1997; Biver et al. 2014; Goesmann et al. 2015; Altwegg et al. 2017; Drozdovskaya et al. 2019).

Both gas-phase and solid-state formation routes of NH_2CHO have been discussed to explain its widespread and abundant detection in the aforementioned star-forming regions. The gas-phase reaction $NH_2 + H_2CO \rightarrow NH_2CHO + H$ has been theoretically suggested to be efficient under interstellar cloud conditions (Barone et al. 2015; Skouteris et al. 2017). However, its reaction rate constant is still under debate (Song & Kästner 2016). In addition, the gas-phase reaction $CO + NH_2 \rightarrow NH_2CO$ and the following, so-called "radical disproportionation" (i.e., $2NH_2CO \rightarrow NH_2CHO + HNCO$) have been reported in early high-temperature studies (150–400°C) simulating the primordial Earth's conditions (Boden & Back 1970; Yokota & Back 1973; Hubbard et al. 1975).

In the solid phase, several low-temperature formation mechanisms of NH_2CHO have been investigated, including atomic addition, radical association with interstellar molecules (e.g., CO, NH_3, and H_2O), and radical–radical recombination reactions. It has been concluded that the successive hydrogenation of isocyanic acid (HNCO) is unlikely to form NH_2CHO on dust grains under interstellar conditions, because

[3] Current address: Laboratory for Astrophysics, Leiden Observatory, Leiden University, P.O. Box 9513, NL-2300 RA Leiden, the Netherlands.
[4] Current address: Istituto Nazionale di Astrofisica, Osservatorio Astronomico di Capodimonte, Salita Moiariello 16, I-80131 Naples, Italy.

of a relatively low rate constant (Song & Kästner 2016). Furthermore, the dual-cyclic mechanism of H-atom abstraction and addition reactions connecting HNCO and NH_2CHO favors the hydrogen-poor species (Haupa et al. 2019). Following the gas-phase work reported in Hubbard et al. (1975), the radical–molecule association of NH_2 + CO resulting in NH_2CO radicals has been adapted to explain the NH_2CHO formation in the energetic processing of CO:NH_3 ice mixture (Hudson & Moore 2000; Bredehoft et al. 2017). However, this pathway is questioned because of the absence of NH_2CO (Jones et al. 2011). Another radical–molecule association route comprising H_2CO and NH_2O has been proposed in Dulieu et al. (2019), but further validation of its efficiency is still desired. As an alternative, barrierless radical–radical recombination of NH_2 and HCO with proper geometric orientation has been suggested to form NH_2CHO in the solid phase (Hudson & Moore 2000). This formation mechanism has also been investigated under different energetic sources, such as fast ions, electrons, and UV, as well as X-ray photons (Jones et al. 2011; Abplanalp et al. 2016; Fedoseev et al. 2016; Ciaravella et al. 2019; Martín-Doménech et al. 2020).

The solid-state chemistry of the CO:NH_3 ice mixture triggered by energetic processing has been extensively investigated in the past decades (Milligan & Jacox 1965; Ferris et al. 1974; Hagen et al. 1979; Grim et al. 1989; Demyk et al. 1998; Hudson & Moore 2000). Although NH_2CHO is a prevalent product detected upon UV photon or ion impacts, the main focii of these studies were more on the spectroscopy of $[NH_4]^+[OCN]^-$ and on the identification of refractory material of biological interests after a relatively long irradiation time. In the last ten years, quantitative studies of the product evolution as a function of energy have become available. For example, Jones et al. (2011) studied the energetic electron bombardment of the CO:NH_3 ice mixture at ∼12 K and reported the temporal profiles of HCO and NH_2CHO to support the suggested reaction pathway, i.e., HCO + $NH_2 \rightarrow NH_2CHO$. More recently, a systematic study showed the dependence of the NH_2CHO formation on the CO:NH_3 ratios and temperatures (10–24 K) upon vacuum UV (VUV) irradiation (Martín-Doménech et al. 2020). The derived kinetics of the NH_2CHO formation was further compared to the formation of the analog product CH_3CHO following similar recombination reactions (CH_3 + CHO) in the CH_4:NH_3 ice mixture and to the data obtained by Jones et al. (2011). It has been concluded that both VUV photons and energetic electrons have very similar effects on the formation cross section of formamide. In spite of these numerous studies, the validity of the proposed solid-state chemistry leading to complex species in an astronomically realistic icy environment comprising abundant H_2O ice is still under debate. More experimental studies are needed in order to understand the role of water in the COM formation, as mentioned in López-Sepulcre et al. (2019). The concern is linked to a higher diffusion barrier of radicals and the limited orientations at the surface and in the bulk ice of H_2O (Enrique-Romero et al. 2019; López-Sepulcre et al. 2019). Agarwal et al. (1985) studied the UV photolysis of interstellar ice containing H_2O, CO, and NH_3 using a relatively high photon fluence. However, they found a list of large prebiotic compounds, with the notable exception of formamide. More recently, Ciaravella et al. (2019) reported the NH_2CHO formation upon X-ray irradiation of an ice mixture with a similar quantity of H_2O, CO, and NH_3 (1:0.9:0.7) at 13 K. Besides this, the potential role of abundant H_2O on the formation kinetics of formamide still remains unclear.

The previous studies mentioned above have devoted great effort into exploring each specific topic, such as OCN^- formation/identification, NH_2CHO formation mechanisms, and kinetics of the newly formed N-bearing products. These topics are important to comprehensively understand the interstellar ice evolution in molecular clouds. However, they have not been experimentally investigated in a single chemical system considering the possible influence of the most abundant H_2O ice. The current laboratory study, for the first time, aims at verifying the formation of NH_2CHO and its chemical derivatives (e.g., HNCO and OCN^-) in CO:NH_3 ice mixtures with or without H_2O triggered by the cosmic ray induced secondary VUV photons (mainly H_2 emissions; Gredel et al. 1989; Cruz-Diaz et al. 2014b). The goal of this study is to reveal a potential chemical network involving the three chemically important species H_2O, CO, and NH_3 in interstellar ice and remove the doubts concerning the COM formation in H_2O-rich ice mantles. The present work is motivated by the importance of NH_2CHO in astrochemistry and highly requested quantitative data regarding the NH_2CHO formation in relevant ice compositions. In this study, the kinetic evolution of all newly formed products, including both N- and O-bearing species, is monitored in situ as a function of photon fluence. The experimental details are described in the next section. The results are presented in Section 3 and discussed in Section 4. The astronomical relevance of the experimental findings and conclusions are summarized in Section 5.

2. Experimental

All experiments have been performed in the Laboratory Astrophysics and Cluster Physics Group in Jena using the ultra-high vacuum (UHV) apparatus. The experimental details have been described in previous work (Potapov et al. 2019), and here only relevant information as well as further modifications are mentioned. The base pressure in the UHV chamber is $\sim 5 \times 10^{-10}$ mbar at room temperature. A copper sample holder is mounted on the tip of a closed-cycle helium cryostat (ColdEdge CS-204) and positioned at the center of the UHV chamber. The temperature at the sample holder monitored by a silicon diode with $\leqslant$0.5 K accuracy can be varied between 10 and 330 K, and is controlled by a resistive heater manipulated by a Lakeshore temperature controller. The thermal contact between the cryostat and the substrate is improved using an indium foil to minimize the temperature difference. In this work, a KBr window, which has a high rate of transmission in the mid-IR range, has been used as a bare substrate that allows the intended ice samples to condense and the bulk ice chemistry triggered by VUV photons at 10 K to be studied.

The VUV photons have been generated by a commercial deuterium lamp (Hamamatsu: H2D2-L11798), a closed-cycle (MgF_2-sealed) light source, and further guided to the ice sample through a MgF_2 UHV viewport installed on the main chamber. The transmission of a MgF2 window decreases from more than ∼88% at 160.0 nm to ∼66% at 121.6 nm (for 2 mm thickness). After calibrating the default emission spectrum provided by the Hamamatsu with the standard transmission of the MgF_2 window, the contribution of Lyα emission in the range of 115–128 nm drops significantly, making it negligible compared to the D_2 emissions at 128–170 nm. The spectral energy distribution with a stronger emission band at ∼160 nm

Table 1
Overview of the Experiments Performed

Exp	T (K)	$N(H_2O)$ (molecules cm^{-2})	$N(CO)$ (molecules cm^{-2})	$N(NH_3)$ (molecules cm^{-2})	Ratio H_2O:CO:NH_3	VUV Fluence (photons cm^{-2})
CO:NH_3+VUV	10	⋯	2.3×10^{16}	3.6×10^{16}	0 : 0.6: 1	8.2×10^{17}
CO:NH_3+VUV	10	⋯	1.4×10^{17}	3.6×10^{16}	0 : 4: 1	8.2×10^{17}
H_2O:CO:NH_3+VUV	10	2.6×10^{17}	1.5×10^{17}	2.9×10^{16}	10 : 5 : 1	8.2×10^{17}
H_2O:CO+VUV	10	2.0×10^{17}	1.5×10^{17}	⋯	1 : 1 : 0	8.2×10^{17}
H_2O:NH_3+VUV	10	3.6×10^{17}	⋯	3.3×10^{16}	10 : 0 : 1	8.2×10^{17}

Table 2
Summary of IR Peak Positions and Band Strength Values Used in This Work

Species	Chemical Formula	IR Peak Position (cm^{-1})	Band Strength (cm $molecule^{-1}$)	References
Carbon monoxide	CO	2137	1.1×10^{-17}	Jiang et al. (1975); Bouilloud et al. (2015)
Ammonia	NH_3	1040	2.0×10^{-17}	Hudson et al. (2022)
Formamide	NH_2CHO	1698	6.5×10^{-17}	Brucato et al. (2006)
Isocyanic acid	HNCO	2261	7.2×10^{-17}	van Broekhuizen et al. (2004)
Cyanate	OCN^-	2150	1.3×10^{-16}	van Broekhuizen et al. (2004)
Formaldehyde	H_2CO	1724	9.6×10^{-18}	Schutte et al. (1993)
Formyl radical	HCO	1855	1.8×10^{-17}	Ryazantsev et al. (2017)
Carbon dioxide	CO_2	2343	1.2×10^{-16}	Gerakines & Hudson (2015)

represents the H_2 Lyman band system induced by cosmic rays interacting with hydrogen molecules in dense molecular clouds (Prasad & Tarafdar 1983; France et al. 2005). The UV photon chemistry induced by the H_2 Werner band system remains for future studies. Although the in situ measurement of UV flux at the sample position is still lacking, a lower photon flux is expected. The estimated UV flux (ϕ) of $\sim 7.6 \times 10^{13}$ photons cm^{-2} s^{-1} has been determined by comparing the formation rate constant (k') of formamide in this work to the averaged formation cross section (σ) value reported in Martín-Doménech et al. (2020), who used the same D_2 lamp under very similar experimental settings: $\phi = k'/\sigma$.

Pure CO (Westfalen, 99.97%) or CO mixed with H_2O vapor (Sigma-Aldrich, UHPLC grade) and NH_3 (Air Liquide, 99.999%) were simultaneously introduced into the main chamber through two separate all-metal leak valves and deposited onto the precooled KBr substrate, which is positioned at an angle of 30° to the deposition tubes and 90° to the IR beam. In order to investigate CO-poor, CO-rich, and H_2O-rich interstellar ices, three different ice compositions were intentionally selected: (1) CO:NH_3 = 0.6:1, (2) CO:NH_3 = 4:1, and (3) H_2O:CO:NH_3 = 10:5:1. The deposited ice mixtures were then irradiated with UV photons at 10 K. The applied ice compositions and column densities are summarized in Table 1.

The growth of the deposited ices and the chemistry induced by the photolysis were monitored in situ using Fourier-transform infrared spectroscopy (FTIR) in transmission mode in a range of 7500–400 cm^{-1} with 1 cm^{-1} resolution. The quantitative analysis of the IR spectra followed the commonly used method described in previous studies (see Jones et al. 2011 and Martín-Doménech et al. 2020) on the formamide formation, and is only briefly explained below. The selected IR absorption peaks were corrected by straight baseline subtraction, and the overlapping peaks were deconvoluted using Gaussian functions, which are both available in the *OriginPro* software. Their corresponding absorption areas were obtained directly by Gaussian curve fitting. The absolute abundances of parent molecules and products were derived by converting IR absorption peak areas to column densities utilizing the modified Beer–Lambert Law (Bennett et al. 2004; Terwischa van Scheltinga et al. 2018),

$$N = \frac{\ln 10 \cdot \int \mathrm{Abs}(\nu) d(\nu)}{A'}, \quad (1)$$

where N is the column density in molecules cm^{-2}, Abs(ν) is the IR absorbance, and A' is the corresponding IR band strength in cm $molecule^{-1}$. The error bars were defined as the standard deviation of the Gaussian fit. This estimation does not account for uncertainties originating from the baseline subtraction procedure and IR absorption band strengths, which have been reported in the literature. The used IR band strengths are summarized in Table 2. The derived column densities of these species can be further refined as soon as more precise values become available.

After VUV irradiation of predeposited (H_2O:)CO:NH_3 ice mixtures for 180 minutes, the photon-processed ice samples were sublimated by a temperature-programmed desorption (TPD) experiment with a ramping rate of 5 K $minute^{-1}$. The desorbed species were analyzed with a quadrupole mass spectrometer (QMS; XT300M, Extorr Inc.). Characteristic desorption temperatures and fragmentation patterns induced by the ionization with 70 eV electrons were recorded in order to identify the newly formed products by comparing them with standard samples in the NIST database and literature. Such a QMS-TPD diagnostic technique has demonstrated a much higher sensitivity with respect to FTIR.

3. Results

3.1. NH_2CHO Formation in CO:NH_3 Ice Mixtures

The top panel of Figure 1 presents the IR absorption spectra of a CO:NH_3 (0.6:1) ice mixture obtained before (a) and after (b) VUV irradiation for 180 minutes at 10 K, as well as that of

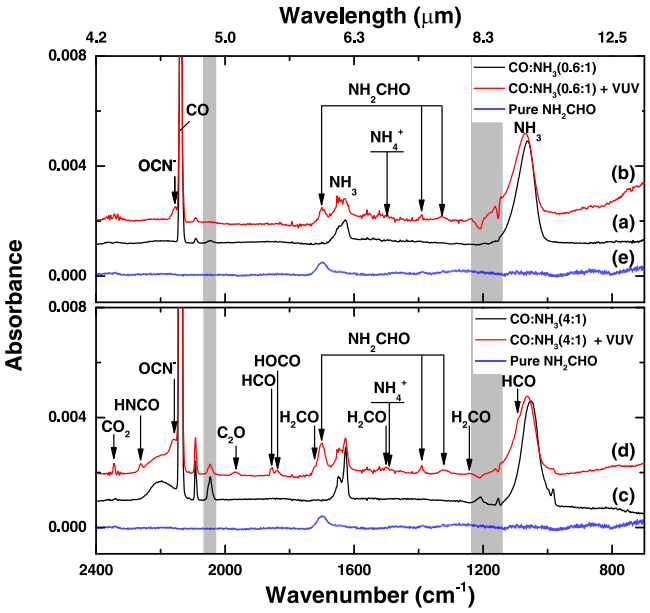

Figure 1. Top panel: IR spectra obtained after deposition of ice mixtures (a) $CO:NH_3$ (0.6:1) and (b) $CO:NH_3$ (0.6:1) after VUV irradiation for a fluence of 8.2×10^{17} photons cm^{-2} (180 minutes) at 10 K. Bottom panel: IR spectra obtained after deposition of (c) $CO:NH_3$ (4:1) and VUV irradiation of (d) $CO:NH_3$ (4:1) ice mixture for a fluence of 8.2×10^{17} photons cm^{-2} (180 minutes). IR spectra are offset for clarity. IR spectrum (e) is shown for pure NH_2CHO ice at 10 K. The shadowed areas are representative for the contamination with Ni $(CO)_4$ from the gas regulator and the FTIR defect features at 2046 and ∼1200 cm^{-1}, respectively (Meunier 2019).

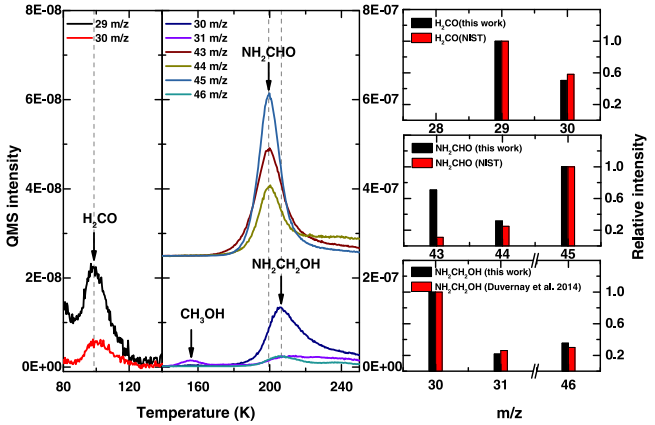

Figure 2. Left: Ion signals obtained during TPD experiment after VUV irradiation of $CO+NH_3$ (4:1) for a fluence of 8.2×10^{17} photons cm^{-2} (180 minutes) at 10 K. Only relevant m/z channels are shown, and they have been shifted for clarity. The dashed lines indicate the peak positions of the corresponding molecules. Right: Comparison of the electron-ionization fragmentation patterns for the QMS-TPD peaks at ∼100, ∼200, and ∼205 K (black) with standard data of H_2CO, NH_2CHO, and NH_2CH_2OH.

(e) pure NH_2CHO as a reference. Besides the absorption features corresponding to the parent molecules, such as CO at 2143 cm^{-1} and NH_3 at 1030 cm^{-1} as well as 1626/1649 cm^{-1} (monomer/aggregate), several IR peaks were only observed upon photolysis of the deposited ice mixture in the spectrum (b), such as the absorption peaks at 1698, 1390, and 1324 cm^{-1} corresponding to C = O stretching (ν_4), C-H bending (ν_6), and C-N stretching (ν_7) modes of NH_2CHO, respectively (King 1971; Torrie & Brown 1994; Brucato et al. 2006; Sivaraman et al. 2013). Other less intense features of NH_2CHO are overlapped with IR peaks of NH_3. The absorption feature at 2155 cm^{-1} is assigned to OCN^- (Demyk et al. 1998; Bernstein et al. 2000; Hudson & Moore 2000; Raunier et al. 2003; van Broekhuizen et al. 2004; Gerakines et al. 2004). Historically, it was labeled as "XCN" in astronomical observations and then successfully identified as the ionic species OCN^- by comparing with laboratory (isotope-labeled) studies (Grim & Greenberg 1987; Schutte & Greenberg 1997). The counterpart cation NH_4^+ is shown at ∼1495 cm^{-1}.

In the bottom panel of Figure 1, the IR absorption spectra of the $CO:NH_3$ (4:1) ice mixture obtained before (c) and after (d) VUV irradiation for 180 minutes at 10 K, as well as that of (e) pure NH_2CHO, are shown. In spectrum (c), the full width at half maximum (FWHM) of the NH_3 symmetric deformation (ν_2) mode becomes more narrow (10%) compared to that in the CO-poor case (spectrum (a)), due to a cage effect of overabundant CO. This is also supported by the observed splitting of the antisymmetric and symmetric deformation modes (ν_4) of the NH_3 monomer. All spectral characteristics clearly suggest that NH_3 resides in the CO-rich ice.

Besides the previously labeled products, several new IR peaks are additionally present in spectrum (d). The IR feature at 2260 cm^{-1} is assigned to HNCO (ν_2), a precursor of OCN^- (Milligan & Jacox 1965; Teles et al. 1989; Lowenthal et al. 2002; van Broekhuizen et al. 2004). The possible isomer cyanate acid (HOCN) is absent, which is consistent with the previous studies suggesting a less efficient isomerization from HNCO to HOCN (Theule et al. 2011; Jiménez-Escobar et al. 2014). The vibrational peaks at 1855 and 1090 cm^{-1} originate from the CO stretching (ν_3) and CH bending (ν_2) modes of HCO, which is the first intermediate product of the CO hydrogenation scheme (Ewing et al. 1960; Milligan & Jacox 1964). The detection of HCO is consistent with the well-known H-atom addition reactions to CO ice, i.e., $CO \rightarrow H_2CO \rightarrow CH_3OH$ (Watanabe & Kouchi 2002a; Fuchs et al. 2009). The strongest C = O (ν_2) vibrational band of H_2CO is clearly observable at 1722 cm^{-1}, along with other relatively weak absorptions at 1500 (ν_3) and ∼1245 (ν_5) cm^{-1} (Khoshkhoo & Nixon 1973; Nelander 1980). The most intense absorption peak of the saturated product CH_3OH (i.e., C–O stretching ν_8) cannot be deconvoluted easily from the broad feature of parent NH_3 around 1030 cm^{-1}. In addition to reactions with free H atoms originating from the NH_3 photolysis, CO is expected to be photoexcited (i.e., $CO \rightarrow CO^*$) and followed by a reaction with another CO, resulting in the formation of CO_2, which is observed at 2343 cm^{-1}. However, this mechanism is considered inefficient compared to the reaction of the hydrocarboxyl radical with atomic hydrogen $HOCO + H \rightarrow CO_2 + 2H$ (Watanabe & Kouchi 2002b; Ioppolo et al. 2011; Chen et al. 2014). Here, we cannot exclude the contribution of this reaction to the CO_2 formation, given the tiny peak of HOCO observed at 1840 cm^{-1}.

The left panel of Figure 2 presents the ion signals, which are obtained during the TPD experiment after VUV irradiation of $CO:NH_3$(4:1) ice at 10 K. Only ion signals at relevant masses are selected to complementarily secure the IR identification. For example, H_2CO is observed through the mass desorption peaks 29 and 30 m/z at ∼100 K, corresponding to the most intense fragment and the molecular mass, respectively. The CH_3OH desorption is demonstrated by the most intense mass fragment of 31 m/z at ∼156 K. The other two desorption peaks at higher temperatures are due to N-bearing species. The peak at ∼200 K (starting from ∼170 K; i.e., 43, 44, and 45 m/z) and

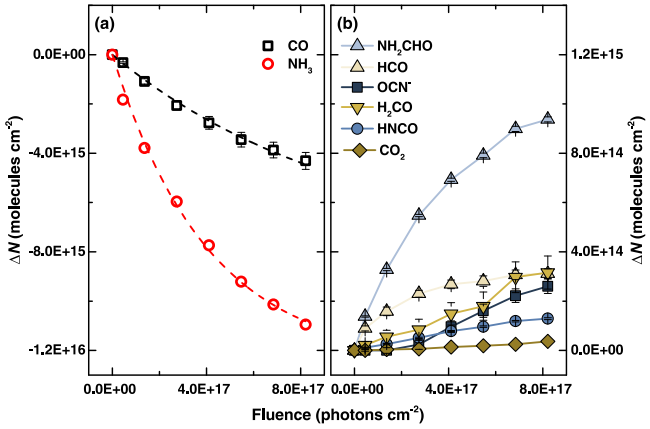

Figure 3. Evolution of (a) parent molecules and (b) newly formed products after VUV irradiation of CO:NH_3 (4:1) ice mixture over a fluence of 8.2×10^{17} photons cm^{-2} (180 minutes). The dashed lines present the fitting results, and the solid lines connecting data are only for clarity.

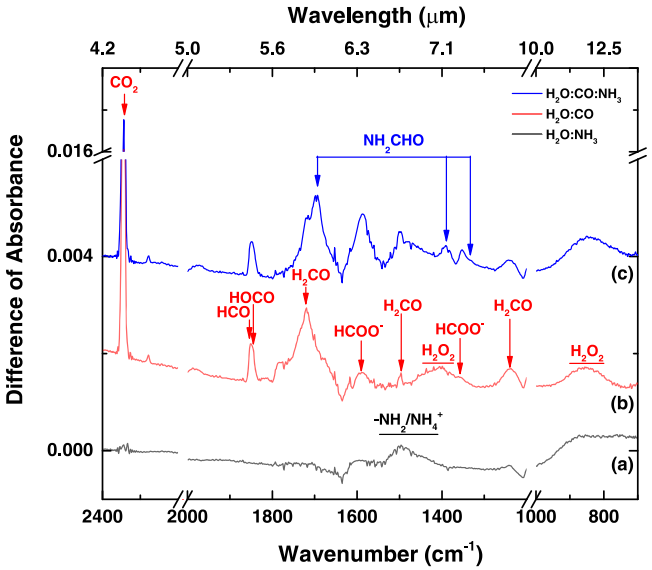

Figure 4. IR difference spectra obtained before and after UV irradiation of (a) H_2O:NH_3 (10:1), (b) H_2O:CO (1:1), and (c) H_2O:CO:NH_3 (10:5:1) ice mixtures for a fluence of 8.2×10^{17} photons cm^{-2} at 10 K. IR spectra are offset for clarity.

the peak at ~205 K (starting from ~180 K; i.e., 30, 31, and 46 m/z) are consistent with the reported desorption temperature of NH_2CHO and NH_2CH_2OH, respectively (Bossa et al. 2009; Ligterink et al. 2018; Martín-Doménech et al. 2020). A somehow different desorption profile has been observed for the mass signal of 43 m/z, which starts increasing at a slightly lower temperature (i.e., ~165 K) than those observed for the mass signals of 44 and 45 m/z. This points to an additional contribution of 43 m/z from HNCO, which is expected to desorb at ~185 K (Fischer et al. 2002; Fedoseev et al. 2015). Furthermore, the identifications are confirmed by comparing their (selected) mass fragmentation patterns induced by electron impact in the right panel of Figure 2. The relative intensities between different mass signals are in good agreement with standard electron (70 eV) ionization patterns as available from the NIST database for H_2CO and NH_2CHO and from the study by Duvernay et al. (2014) for NH_2CH_2OH, except for the 43 m/z, which has contributions from both HNCO and NH_2CHO. The experimental results from the ion signals during the TPD experiment support the IR-spectral assignments of H_2CO and NH_2CHO and further point out the possible formation of their saturated derivatives such as CH_3OH and NH_2CH_2OH, whose IR vibrational features might largely overlap with their precursors and whose intensities are below the FTIR detection limits.

3.2. Kinetic Evolution of CO:NH_3 Ice Mixture under VUV Irradiation

In addition to the qualitative identifications of the photolysis products, the absolute column density (N) of the parent molecules and newly formed species were monitored in situ as a function of photon fluence. In Figure 3, the evolutions of parent molecules (e.g., CO and NH_3 in Figure 3(a)) and major products (e.g., NH_2CHO, HCO, OCN^-, H_2CO, HNCO, and CO_2 in Figure 3(b)) after VUV irradiation of the CO:NH_3 (4:1) ice (fluence of 8.2×10^{17} photons cm^{-2}) are shown. The consumption of CO and NH_3 is fit by a single exponential equation:

$$\Delta N(\text{molecules}) = \alpha(1 - \exp(\sigma \cdot \phi \cdot t)), \quad (2)$$

where α is the saturation value (i.e., the maximum change when reaching the equilibrium state) in molecules cm^{-2}, σ is the photolysis cross section in cm^2 $photon^{-1}$, ϕ is the UV flux in photons cm^{-2} s^{-1}, and t is the irradiation time in seconds. The derived cross-section values are $(1.0 \pm 0.2) \times 10^{-18}$ and $(2.5 \pm 0.2) \times 10^{-18}$ cm^2 $photon^{-1}$ for CO and NH_3, respectively. The value of NH_3 is larger than that of CO, due to the direct photodissociation of NH_3 forming NH_2 and H.

In Figure 3(b), NH_2CHO and HCO are the two products that form most efficiently at the beginning of VUV irradiation. The abundances of NH_2CHO and HCO increase rapidly up to a fluence of 2.7×10^{17} photons cm^{-2}. The formation cross-section values of NH_2CHO and HCO are $(2.9 \pm 0.2) \times 10^{-18}$ and $(6.0 \pm 0.7) \times 10^{-18}$ cm^2 $photon^{-1}$, respectively. Once the HCO production rate slows down, a similar saturation behavior is also observed in NH_2CHO. The obtained ratio of NH_2CHO/HCO shows a relatively constant value of 2.7 ± 0.2 after reaching a fluence of 2.7×10^{17} photons cm^{-2}, implying a chemical correlation between these two. The formation of H_2CO and HNCO is also observed upon VUV processing, but with much lower production yields compared to NH_2CHO. Unlike the aforementioned species, the production of OCN^- and CO_2 is considered as a high-order generation of photolysis products, given the different kinetic curves and the delay of formation. The abundances were only detectable after reaching a fluence of 2.7×10^{17} photons cm^{-2}. However, at the end of the photolysis experiment, the absolute column density of OCN^- was higher than that of HNCO. Similar product evolution as a function of photon fluence was also found in the CO:NH_3 (0.6:1) ice mixture for NH_2CHO, H_2CO, and OCN^-, but their intermediate products HCO and HNCO were absent.

3.3. NH_2CHO Formation in H_2O-rich Ice Mixture

Figure 4 shows the difference IR absorption spectra before and after 180 minutes VUV irradiation of (a) H_2O:NH_3 (10:1), (b) H_2O:CO (1:1), and (c) H_2O:CO:NH_3 (10:5:1) ice mixtures at 10 K. The newly formed products are present in positive peaks and the parent molecules are present in negative features, which are intentionally omitted in Figure 4, except for H_2O at

$\sim$1633 cm^{-1}. The control experiments (a) H_2O:NH_3 (10:1) and (b) H_2O:CO (1:1) provide spectral evidence to identify possible carriers of the newly formed peaks, which are exclusively detected in the H_2O:CO:NH_3 ice mixture (spectrum (c) in Figure 4).

As shown in spectrum (a), VUV photolysis of H_2O:NH_3 ice mixture only results in a broad N–H bending feature around 1497 cm^{-1}, which has been assigned to NH_2 and/or NH_4^+ in $[NH_4]^+[OH]^-$ salt (Schutte et al. 1999; Zheng et al. 2008). The peaks of the possible product (NH_2OH) originating from OH + NH_2 are absent. This is probably due to a low formation yield or high destruction cross section of NH_2OH upon VUV-photon impact (Fedoseev et al. 2015). In spectrum (b), the new IR features are assigned to C-bearing species appearing upon VUV irradiation of H_2O:CO. Besides CO_2, H_2CO is another C-bearing product, presenting absorption bands at 1719, 1498, and 1244 cm^{-1}. The IR features of the intermediate radicals HCO and HOCO (i.e., the precursors of H_2CO and CO_2, respectively) are largely overlapped, as shown at $\sim$1853/1846 cm^{-1} (Milligan & Jacox 1971; Bennett et al. 2010). The spectral deconvolution of these two peaks was realized by Gaussian curve fitting and further confirmed during the TPD experiment because these two species have different desorption temperatures (IR absorptions at 1853 and 1846 cm^{-1} disappeared at 15–30 and 30–45 K, respectively). The IR features of the formate anion ($HCOO^-$) are visible at 1587 and 1355 cm^{-1} (Milligan & Jacox 1971; Bennett et al. 2010). This suggests a possible acid–base reaction between HCOOH and H_2O (Schutte et al. 1999; Hudson & Moore 2000). All aforementioned features shown in spectra (a) and (b) are also unambiguously present in spectrum (c) of the VUV irradiated H_2O:CO:NH_3 (10:5:1) ice mixture. In addition, the newly appeared IR features present in spectrum (c) must be attributed to photolysis products containing CN bonds; the IR peaks at 1693, 1392, and 1333 cm^{-1} have been assigned to NH_2CHO. However, OCN^- or HNCO, the chemical derivatives of NH_2CHO, are absent.

The kinetic analysis shows that NH_2CHO is one of the first-generation products and is observed in all studied CO:NH_3 ice mixtures with or without the presence of H_2O. The evolution of $N(NH_2CHO)$ normalized by the initial parent species (i.e., $N_0(NH_3)$) as a function of photon fluence and the fit according to Equation (2) are shown in Figure 5(a). The corresponding values of the fitting, such as the saturation α (unitless) and the formation cross section σ (cm^2 photon^{-1}) are presented in Figures 5(b) and (c), respectively. It is important to note that the derived fitting outcomes are only considered as effective results that represent the combination of product's formation and destruction channels. The photon-induced cross-section values (σ) that indicate the efficiency of reaching the steady state are $(3.6 \pm 0.4) \times 10^{-18}$, $(2.9 \pm 0.2) \times 10^{-18}$, and $(0.8 \pm 0.1) \times 10^{-18}$ cm^2 photon^{-1} for CO:NH_3 (0.6:1), CO:NH_3 (4:1), and H_2O:CO:NH_3 (10:5:1) ice mixtures, respectively. Although a relatively low formation cross section was obtained for the H_2O-rich experiment, the highest saturation value (α) of 0.10 ± 0.01 was found in the H_2O:CO:NH_3 (10:5:1) ice. In the CO:NH_3 (4:1) and CO:NH_3 (0.6:1) experiments, these values are considerably smaller, i.e., 0.028 ± 0.001 and 0.001 ± 0.001, respectively. The experimental results suggest that the NH_2CHO formation is strongly influenced by initial ice compositions and by the number of photons absorbed in the bulk ice. Ice mixtures, which are H_2O-

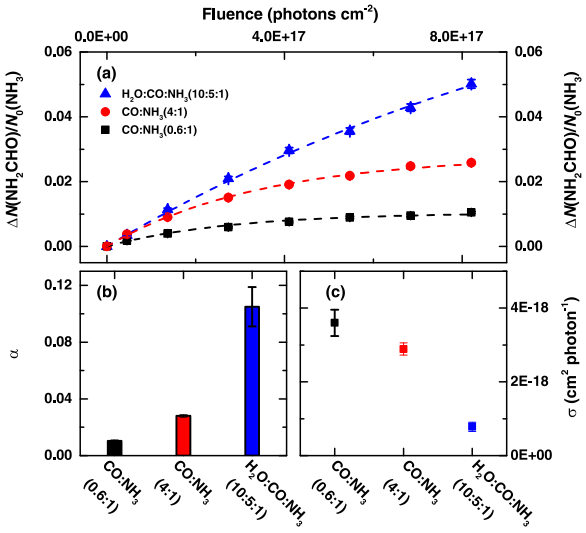

Figure 5. Upper panel: (a) Abundance evolution of the newly formed NH_2CHO in the VUV photolysis of three investigated ice mixtures: CO:NH_3 (0.6:1), CO:NH_3 (4:1), and H_2O:CO:NH_3 (10:5:1), over a fluence of 8.2×10^{17} photons cm^{-2}. The dashed lines present the best fitting. Bottom panel: The derived fitting values of (b) saturation, α, and (c) formation cross section, σ, for NH_2CHO are present for three investigated CO:NH_3 ice mixtures

or CO-rich, may play an important role in preventing the NH_2CHO destruction by absorbing incoming photons. Moreover, UV irradiation of H_2O ice can also lead to the formation of mobile (nonthermal) H atoms that can diffuse in the bulk ice and chemically convert photofragments, such as NHCHO or NH_2CO, back to NH_2CHO. The shielding from further destruction explains the absence of HNCO and OCN^- in the H_2O:CO:NH_3 (10:5:1) experiment and enhances the NH_2CHO abundance as shown in Figure 5(a).

4. Discussion

In this work, since there are two MgF_2 windows between the ice sample and the UV-photon source, the photon energy distribution is mainly characterized by $\sim$160 nm ($\sim$79%) with a tiny contribution from Lyα ($\sim$6%) as mentioned in the Experimental section. Therefore, the ionization of NH_3 by photons having an energy above 10 eV (i.e., <124 nm) is minimal compared to the photodissociation of NH_3. We only focus on the ice chemistry originating from reactions between neutral radicals in solid state in the following discussion. The possible ion/electron chemistry induced by photoionization in binary ice containing NH_3 is much more complex and has been experimentally investigated by Demyk et al. (1998) and Hudson & Moore (2000). On the other side, the direct photodissociation of CO is forbidden due to the higher threshold energy required (i.e., 11.09 eV). However, CO has relatively strong absorption cross-section values (up to $\sim 1.5 \times 10^{-17}$ cm^2 photon^{-1}) in the range of 127–157 nm coinciding with the molecular (D_2/H_2) emission ($\sim$130–165 nm). These photons can excite some CO molecules into the first electronically excited state ($A^1\Pi \leftarrow X^1\Sigma^+$; CO*), which carries excess energy of up to 7.9 eV (Lu et al. 2005; Mason et al. 2006; Cruz-Diaz et al. 2014b). In contrast, NH_3, with a much lower threshold energy of 4.4 eV, is expected to be efficiently dissociated upon the impact of VUV photons, resulting in amino radicals (NH_2) and H atoms via the

dissociation reaction (Okabe & Lenzi 1967):

$$NH_3 \xrightarrow{+h\nu} NH_2 + H. \quad (3)$$

Therefore, in a CO:NH_3 ice mixture, the consumption of CO is through either the so-called nonthermal desorption following the photon energy transfer from CO^* to surface CO or chemical reactions with H atoms or NH_2 in the ice. For example, the interactions between CO and H atoms has been proposed to form HCO via H-atom addition reactions (Watanabe & Kouchi 2002a):

$$CO + H \rightarrow HCO. \quad (4)$$

The newly formed HCO can immediately recombine with surrounding NH_2 radicals, resulting in NH_2CHO via the radical–radical recombination:

$$HCO + NH_2 \rightarrow NH_2CHO. \quad (5)$$

In addition, the successive hydrogenation of HCO could also take place, forming H_2CO:

$$HCO + H \rightarrow H_2CO. \quad (6)$$

The two HCO consumption channels (i.e., reactions (5) and (6)) compete with each other. However, reaction (5) can occur when HCO and NH_2 radicals are nearby, and reaction (6) requires additional H atoms from another NH_3 photodissociation. Therefore, the formamide route is favored under the current experimental conditions and the derived ratio of $N(NH_2CHO)/N(H_2CO)$ is >3 at steady state in all CO:NH_3 experiments. For each NH_3 dissociation event, one may expect that, after CO hydrogenation (reaction (4)), NH_2 is the only radical near the newly formed HCO. The prompt recombination following reaction (5) is expected without further diffusion. The second H atom requires the photodissociation of another NH_3 and additional diffusion. It is important to note that radical–radical recombination reactions could also lead back to NH_3 and CO through the direct H transfer (Enrique-Romero et al. 2019). However, the repetitive NH_3 dissociation followed by the CO hydrogenation effectively favors the formation of formamide.

Besides interactions between radicals and ground-state molecules, a fraction of electronically excited carbon monoxide (CO^*) can directly react with NH_2 radicals followed by H-atom recombination, providing an additional formation pathway to NH_2CHO through the reactions:

$$CO^* + NH_2 \rightarrow NH\_2CO \quad (7)$$

and

$$NH_2CO + H \rightarrow NH_2CHO. \quad (8)$$

A higher activation barrier reported for reaction (7) with respect to that of reaction (4) (i.e., 15 kJ mol^{-1} versus 8 kJ mol^{-1}, in the gas phase) can be easily compensated by the absorbed VUV-photon energy. However, if NH_2CO is formed as an intermediate product, it is strongly expected to be converted backward, forming HNCO (Noble et al. 2015; Haupa et al. 2019).

The chemistry of electronically excited CO with other strongly bound molecules, such as H_2 and N_2, with high activation barriers has been experimentally investigated in the solid state by Chuang et al. (2018) and Martín-Doménech et al. (2020). The interactions between CO^* and NH_3 might also be relevant in the present study. However, the presence of available CO^* in the ice mixture strongly depends on the impacting photon fluence and the timescale of energy dissipation in the bulk ice. Additionally, the direct proton transfer from NH_3 to CO could also contribute to the formation of NH_2CHO, given that the reaction barrier of 314.5 kJ mol^{-1} calculated in current work for the isolated CO–NH_3 complex at the b3lyp/6-311G+(d,p) level can be easily overcome by the absorption of photons. Despite the nondetection of the vibrational feature of the CO–NH_3 complex (~2145 cm^{-1}; Lundell et al. 1998), this formation route cannot be excluded.

The continued UV irradiation leads to further chemical modification of first-generation products. For example, the photolysis of NH_2CHO results in the HNCO formation through the H_2 loss channel (Lundell et al. 1998; Duvernay et al. 2005):

$$NH_2CHO \xrightarrow{+h\nu} HNCO + H_2. \quad (9)$$

A very similar photodissociation of H_2CO is also expected, enriching the content of reactive radicals like HCO, H, or even CO. Moreover, the dehydrogenation pathway through H-atom abstraction reactions has also been reported via (Haupa et al. 2019; Suhasaria & Mennella 2020)

$$NH_2CHO \xrightarrow{+H(-H_2)} NH_2CO \xrightarrow{+H(-H_2)} HNCO. \quad (10)$$

The product HNCO can react with the surrounding NH_3 ice and convert into OCN^-, through the acid–base reaction:

$$HNCO + NH_3 \leftrightarrow [NH_4]^+[OCN]^-. \quad (11)$$

This is supported by observing a delay of the OCN^- formation shown in Figure 3. The efficient conversion from the neutral isocyanic acid (HNCO) to the cyanate ion (OCN^-) has been experimentally confirmed at 10 K (Jiménez-Escobar et al. 2014).

These secondary products (e.g., HNCO and OCN^-) are absent in the photolysis of the H_2O-rich ice mixture (H_2O:CO:NH_3 = 10:5:1). Instead, the abundance of NH_2CHO rapidly increases with photon fluence. NH_2CHO, which is formed by either reactions (4)–(5) or (7)–(8), is largely preserved in H_2O ice instead of being photodissociated into simpler products.

In addition to the formation of dehydrogenated species, H_2CO could also be hydrogenated into saturated molecules through successive addition reactions of H atoms:

$$H_2CO \xrightarrow{+2H} CH_3OH. \quad (12)$$

However, hydrogenation of NH_2CHO forming NH_2CH_2OH has been shown to be less likely (Noble et al. 2015). Since aminomethanol is only tentatively observed in the QMS-TPD data, its formation could originate from the thermal chemistry (Duvernay et al. 2014):

$$NH_3 + H_2CO \rightarrow NH_2CH_2OH. \quad (13)$$

As a consequence of the H_2O dissociation, some OH radical association reactions might take place as well. The interaction between OH radicals and CO is expected to result in the intermediate product HOCO through a barrierless reaction:

$$OH + CO \rightarrow HOCO. \quad (14)$$

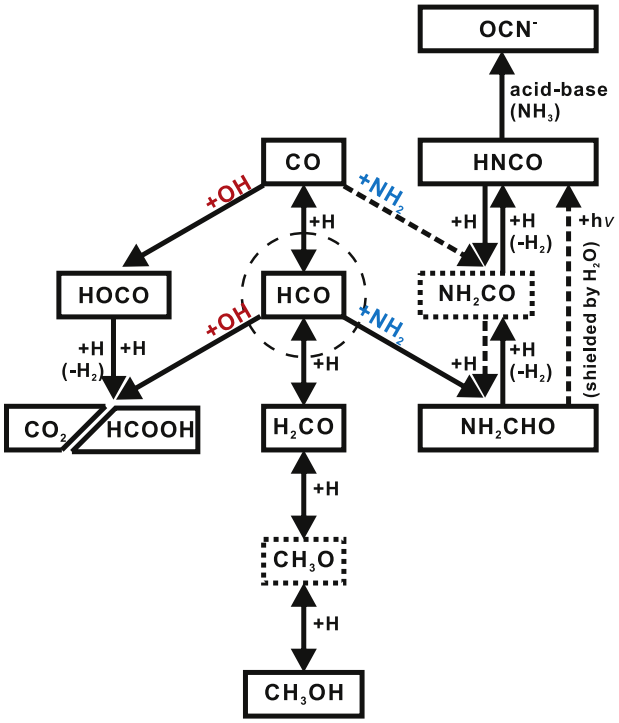

Figure 6. Proposed reaction diagram linking interstellar simple molecules and the newly formed N-bearing COMs formed at 10 K under VUV irradiation of H_2O:CO:NH_3 ice mixtures. The dashed boxes represent undetected intermediate species.

The hydrogenation of HOCO leads to the formation of CO_2 and HCOOH (Ioppolo et al. 2011; Qasim et al. 2019):

$$\mathrm{HOCO} + \mathrm{H} \rightarrow \mathrm{CO_2} + \mathrm{H_2} \quad (15a)$$

and

$$\mathrm{HOCO} + \mathrm{H} \rightarrow \mathrm{HCOOH}. \quad (15b)$$

Alternatively, HCOOH is also formed through the recombination of HCO with OH radicals:

$$\mathrm{HCO} + \mathrm{OH} \rightarrow \mathrm{HCOOH}. \quad (16)$$

A similar acid–base reaction has also been reported for a HCOOH ice mixed with H_2O- or NH_3-rich environments, leading to ionic species (Schutte et al. 1999; Hudson & Moore 2000; Bergner et al. 2016):

$$\mathrm{HCOOH} + \mathrm{H_2O(or NH_3)} \rightarrow [\mathrm{HCOO}]^-[\mathrm{H_3O}]^+(\mathrm{or}[\mathrm{NH_4}]^+). \quad (17)$$

The proposed reactions induced by VUV irradiation of astronomically relevant ice mixtures containing H_2O, CO, and NH_3 are summarized in Figure 6.

5. Astrochemical Implications and Conclusions

The present laboratory study demonstrates the solid-state chemistry of forming NH_2CHO and its derivatives, including HNCO and $[OCN]^-[NH_4]^+$, by the VUV photolysis of CO:NH_3 ice mixtures at 10 K. We investigated the proposed formation mechanism involving HCO radicals and NH_2 radicals in two different interstellar-relevant ice compositions in molecular clouds: H_2O-rich and CO-rich ice analogs. The parent molecules and newly formed products were monitored in situ by IR spectroscopy as a function of photon fluence and complementarily confirmed by mass spectrometry during the TPD experiments. Besides the identifications of the first-generation products in both ice scenarios, the further interactions between NH_2CHO and energetic H atoms triggered by continuous VUV irradiation result in hydrogen-poor HNCO (or OCN^- when reacting with NH_3). The kinetic analysis of N-bearing products offers a hint at the solid-state chemical network from the most abundant species (H_2O, CO, CO_2, and NH_3) after energetic processing in molecular clouds before evaporation.

In the early stage of molecular clouds ($1 \leqslant A_V \leqslant 5$), the gas density increases to $10^4\,\mathrm{cm^{-3}}$, leading to a decrease of the cloud temperature down to ~20 K. Atomic reactions are considered to dominate the surface chemistry on submicron-sized interstellar dust grains. For example, in translucent clouds ($A_V \geqslant 3$), H atoms and O atoms diffuse on the surfaces of dust grains, forming H_2O ice via the reactions $\mathrm{O} \xrightarrow{+\mathrm{H}} \mathrm{OH} \xrightarrow{+\mathrm{H}} \mathrm{H_2O}$. This occurs along with other H-atom addition reactions to N and C atoms, leading to NH_3 and CH_4, respectively (Hidaka et al. 2011; Fedoseev et al. 2015; Qasim et al. 2020). In the meantime, a fraction of gaseous CO is also expected to participate in the first H_2O-rich ice chemistry, leading to CO_2 formation (Ioppolo et al. 2011). As the gas density continuously increases in dense clouds, the temperature of the dust grains drops further (i.e., there is a negative correlation between A_V and temperature; Hocuk et al. 2017), allowing more CO to condense onto the previous H_2O-rich ice layer. This is the so-called "CO catastrophic freeze-out stage," forming a second CO-rich ice layer (Boogert et al. 2015). With the significantly increased lifetime of H atoms on surfaces, the H-atom addition reactions play an essential role in converting inorganic CO into (complex) organic species, such as aldehydes and alcohols (Watanabe & Kouchi 2002a; Fuchs et al. 2009; Chuang et al. 2016, 2017; Fedoseev et al. 2017; Simons et al. 2020). The accumulation of interstellar ice is expected to take place within 10^5 yr, based on theoretical estimations (i.e., $10^9/n_{(\mathrm{H})}$, where $n_{(\mathrm{H})} = 10^4\,\mathrm{cm^{-3}}$; see Willacy & Millar 1998). Besides the surface chemistry dominated by atom(radical)–molecule reactions, the cosmic rays (CR) and the secondary UV photons induced by CR interacting with H_2 have been proven to act as efficient chemical triggers to facilitate the molecular complexity in the ice mantles in the remaining 10^5–10^7 yr, as the typical lifetime of molecular cloud has been estimated up to ~10^7 yr (Chevance et al. 2020). Considering higher penetration depths of UV or CRs than the thickness of ice mantles, in contrast to atoms, these energetic sources can efficiently trigger the bulk ice chemistry involving the preserved molecules in the deep ice mantles, both in H_2O-rich and CO-rich ice layers (Cruz Diaz et al. 2014a; Cruz-Diaz et al. 2014b).

The investigated photochemistry of ices leading to N-bearing organic species is expected to take place in different astronomically relevant ice layers. The applied UV fluence is comparable to the accumulated UV photons in molecular clouds, i.e., $3 \times 10^{17-18}$ photons $\mathrm{cm^{-2}}$ assuming a UV flux of 10^{3-4} photons $\mathrm{cm^{-2}\,s^{-1}}$ and a cloud lifetime of 10^7 yr (Prasad & Tarafdar 1983; Cecchi-Pestellini & Aiello 1992; Shen et al. 2004). In the H_2O-rich ice mixture, the interactions between CO and H_2O photofragments (e.g., OH radicals and H atoms) mainly contributed to the formation of C-bearing species, providing additional chemical routes to enrich the abundance of CO_2, H_2CO, $HCOOH/HCOO^-$, HCO, and HOCO in H_2O ices besides (non-energetic) atom addition reactions. The only N-bearing species formed in the ice was NH_2CHO. HNCO (or

OCN^-) was not observed, suggesting that the newly formed NH_2CHO was most likely protected in the H_2O-rich environment. The experimental findings demonstrate that the NH_2CHO formation pathway proposed for the photolysis of $CO:NH_3$ ice mixtures is still valid in interstellar H_2O-rich ice layers. Apparently, the binding/diffusing energy of radicals in H_2O-rich ice can be overcome in the UV-photon induced ice chemistry. Moreover, this reaction channel takes place simultaneously with other reactions, such as $CO+2H \rightarrow H_2CO$ and $CO+OH \rightarrow HOCO$, induced by VUV-photons. In the interstellar CO-rich ice layer, the UV-photon induced production of C-bearing species is limited due to the scarcity of H_2O photofragments. CO_2 and H_2CO are minor products. Their precursor species, such as HCO and HOCO, are trapped in CO ice. The N-bearing products include NH_2CHO, HNCO, and OCN^-.

In astronomical observations, the vibrational feature of OCN^- (4.64 μm) was first detected in the solid phase by Lacy et al. (1984) and later identified by Demyk et al. (1998). The correlation between HNCO and OCN^- has been established (Hudson & Moore 2000; Jiménez-Escobar et al. 2014). The present laboratory study also supports the chemical link between these two species at low temperatures without thermal processing. The absence of HNCO in the interstellar H_2O-rich ice probably implies fast acid–base reactions involving a proton transfer, which may not be limited to NH_3. An attempt to search for the solid-state IR absorption features of NH_2CHO has been reported by Schutte et al. (1999) and Raunier et al. (2004), but resulted in only a tentative identification. However, NH_2CHO and its chemical derivative HNCO have been detected simultaneously in cometary material, which is believed to inherit the most pristine ice species in molecular clouds (Biver et al. 2014; Altwegg et al. 2017). Future observation of N-bearing organic molecules, including NH_2CHO and its (de-)hydrogenated species (e.g., HNCO and NH_2CH_2OH) in interstellar ice mantles using the JWST is desired in order to reveal the full chemical fingerprints of N-bearing species in star-forming regions. Astronomical observations show a strong abundance correlation between HNCO and NH_2CHO in star-forming regions (see Figure 1 in López-Sepulcre et al. 2019). The chemical transformation from NH_2CHO to HNCO has been found in this work. However, the derived ratio of $NH_2CHO/HNCO > 1$, which is in contradiction to observations, suggests that there are additional destruction routes, such as H-atom abstraction, high-energetic photons, and cosmic ray dissociation, influencing products' degree of hydrogenation. This work acts as a case study on the UV photolysis of interstellar ice analogs containing $CO:NH_3$ in an H_2O-rich environment. A systematic comparison of the conversion rate between NH_2CHO and HNCO induced by different (non-)energetic sources is highly desired to better understand the full interstellar ice evolution.

In conclusion, based on the experimental results on the photolysis chemistry of $CO:NH_3$ ice mixtures in H_2O-rich and CO-rich ice analogs, the main findings of this work can be summarized as below:

1. VUV irradiation of $CO:NH_3$ ice mixtures in H_2O-rich and CO-rich environments at 10 K shows an efficient formation pathway leading to N-bearing molecules (NH_2CHO, HNCO, and OCN^-) under molecular cloud conditions.
2. The formation kinetics of NH_2CHO in H_2O-rich and CO-rich ice are derived (Figure 5). It shows a strong dependency on the initial ice compositions. The highest production yield of NH_2CHO is observed in the H_2O-rich ice mixture.
3. NH_2CHO is reported as a first-generation product of $CO:NH_3$ ice mixtures upon VUV irradiation. The continuous photon impact or the photon-induced formation of free (energetic) H atoms from H_2O and NH_3 can further influence the final product composition including the formation of HNCO and OCN^-.

Th.H. acknowledges support from the European Research Council under the Horizon 2020 Framework Program via the ERC Advanced Grant Origins 83 24 28. Authors thank the Leiden Ice Database for Astrochemistry (LIDA) for providing the solid-state IR spectrum of formamide.

ORCID iDs

K.-J. Chuang https://orcid.org/0000-0001-6877-5046
C. Jäger https://orcid.org/0000-0001-7803-0013
S. A. Krasnokutski https://orcid.org/0000-0002-9816-3187
D. Fulvio https://orcid.org/0000-0002-7260-9742
Th. Henning https://orcid.org/0000-0002-1493-300X

References

Abplanalp, M. J., Gozemc, S., Krylovc, A. I., et al. 2016, PNAS, 113, 7727
Agarwal, V. K., Schutte, W., Greenberg, J. M., et al. 1985, OrLi, 16, 21
Altwegg, K., Balsiger, H., Berthelier, J. J., et al. 2017, MNRAS, 469, S130
Altwegg, K., Balsiger, H., & Fuselier, S. A. 2019, ARA&A, 57, 113
Barks, H. L., Buckley, R., Grieves, G. A., et al. 2010, ChemBioChem, 11, 1240
Barone, V., Latouche, C., Skouteris, D., et al. 2015, MNRAS, 453, L31
Bennett, C. J., Hama, T., Kim, Y. S., Kawasaki, M., & Kaiser, R. I. 2010, ApJ, 727, 27
Bennett, C. J., Jamieson, C., Mebel, A. M., & Kaiser, R. I. 2004, PCCP, 6, 735
Bergner, J. B., Öberg, K. I., Rajappan, M., & Fayolle, E. C. 2016, ApJ, 829, 85
Bernstein, M., Sandford, S., & Allamandola, L. 2000, ApJ, 542, 894
Bisschop, S. E., Jørgensen, J. K., van Dishoeck, E. F., & de Wachter, E. B. M. 2007, A&A, 465, 913
Biver, N., Bockelée-Morvan, D., Debout, V., et al. 2014, A&A, 566, L5
Bockelee-Morvan, D., Wink, J., Despois, D., et al. 1997, EM&P, 78, 67
Boden, J., & Back, R. 1970, Trans. Faraday Soc., 66, 175
Boogert, A. C. A., Gerakines, P. A., & Whittet, D. C. B. 2015, ARA&A, 53, 541
Bossa, J., Theule, P., Duvernay, F., & Chiavassa, T. 2009, ApJ, 707, 1524
Bouilloud, M., Fray, N., Bénilan, Y., et al. 2015, MNRAS, 451, 2145
Bredehoft, J. H., Bo?hler, E., Schmidt, F., Borrmann, T., & Swiderek, P. 2017, ESC, 1, 50
Brucato, J. R., Baratta, G. A., & Strazzulla, G. 2006, A&A, 455, 395
Cecchi-Pestellini, C., & Aiello, S. 1992, MNRAS, 258, 125
Chen, Y.-J., Chuang, K.-J., Muñoz Caro, G. M., et al. 2014, ApJ, 781, 15
Chevance, M., Kruijssen, J. D., Hygate, A. P. S., et al. 2020, MNRAS, 493, 2872
Chuang, K.-J., Fedoseev, G., Ioppolo, S., van Dishoeck, E. F., & Linnartz, H. 2016, MNRAS, 455, 1702
Chuang, K.-J., Fedoseev, G., Qasim, D., et al. 2017, MNRAS, 467, 2552
Chuang, K.-J., Fedoseev, G., Qasim, D., et al. 2018, A&A, 617, A87
Ciaravella, A., Jiménez-Escobar, A., Cecchi-Pestellini, C., et al. 2019, ApJ, 879, 21
Colzi, L., Rivilla, V., Beltrán, M., et al. 2021, A&A, 653, A129
Coutens, A., Jørgensen, J., Van der Wiel, M., et al. 2016, A&A, 590, L6
Cruz Diaz, G. A., Muñoz Caro, G. M., Chen, Y.-J., & Yih, T.-S. 2014a, A&A, 562, A120
Cruz-Diaz, G. A., Muñoz Caro, G. M., Chen, Y.-J., & Yih, T.-S. 2014b, A&A, 562, A119
Demyk, K., Dartois, E., d'Hendecourt, L., et al. 1998, A&A, 339, 553
Drozdovskaya, M. N., van Dishoeck, E. F., Rubin, M., Jørgensen, J. K., & Altwegg, K. 2019, MNRAS, 490, 50

Dulieu, F., Nguyen, T., Congiu, E., Baouche, S., & Taquet, V. 2019, MNRASL, 484, L119
Duvernay, F., Danger, G., Theulé, P., Chiavassa, T., & Rimola, A. 2014, ApJ, 791, 75
Duvernay, F., Trivella, A., Borget, F., et al. 2005, JPCA, 109, 11155
Enrique-Romero, J., Rimola, A., Ceccarelli, C., et al. 2019, ESC, 3, 2158
Ewing, G. E., Thompson, W. E., & Pimentel, G. C. 1960, JChPh, 32, 927
Fedoseev, G., Chuang, K.-J., Ioppolo, S., et al. 2017, ApJ, 842, 52
Fedoseev, G., Chuang, K.-J., van Dishoeck, E. F., Ioppolo, S., & Linnartz, H. 2016, MNRAS, 460, 4297
Fedoseev, G., Cuppen, H. M., Ioppolo, S., Lamberts, T., & Linnartz, H. 2015, MNRAS, 448, 1288
Fedoseev, G., Ioppolo, S., Zhao, D., Lamberts, T., & Linnartz, H. 2015, MNRAS, 446, 439
Ferris, J., Williams, E., Nicodem, D., HUBBARD, J. S., & VOECKS, G. E. 1974, Natur, 249, 437
Fischer, G., Geith, J., Klapötke, T. M., & Krumm, B. 2002, Zeitschrift für Naturforschung B, 57, 19
France, K., Andersson, B., McCandliss, S., & Feldman, P. 2005, ApJ, 628, 750
Fuchs, G. W., Cuppen, H. M., Ioppolo, S., et al. 2009, A&A, 505, 629
Fulvio, D., Potapov, A., He, J., & Henning, T. 2021, Life, 11, 568
Gerakines, P., Moore, M., & Hudson, R. 2004, Icar, 170, 202
Gerakines, P. A., & Hudson, R. L. 2015, ApJL, 808, L40
Goesmann, F., Rosenbauer, H., Bredehöft, J. H., et al. 2015, Sci, 349, aab0689
Gredel, R., Lepp, S., Dalgarno, A., & Herbst, E. 1989, ApJ, 347, 289
Grim, R. J., & Greenberg, J. M. 1987, ApJL, 321, L91
Grim, R. J. A., Greenberg, J. M., de Groot, M. S., et al. 1989, A&AS, 78, 161
Hagen, W., Allamandola, L., & Greenberg, J. 1979, Ap&SS, 65, 215
Halfen, D., Ilyushin, V., & Ziurys, L. 2011, ApJ, 743, 60
Haupa, K. A., Tarczay, G., & Lee, Y.-P. 2019, JACS, 141, 11614
Herbst, E. 2017, IRPC, 36, 287
Herbst, E., & van Dishoeck, E. F. 2009, ARA&A, 47, 427
Hidaka, H., Watanabe, M., Kouchi, A., & Watanabe, N. 2011, PCCP, 13, 15798
Hocuk, S., Szűcs, L., Caselli, P., et al. 2017, A&A, 604, A58
Hubbard, J., Voecks, G., Hobby, G., et al. 1975, JMolE, 5, 223
Hudson, R., & Moore, M. 2000, A&A, 357, 787
Hudson, R. L., Gerakines, P. A., & Yarnall, Y. Y. 2022, ApJ, 925, 156
Imai, M., Sakai, N., Oya, Y., et al. 2016, ApJL, 830, L37
Ioppolo, S., Fedoseev, G., Chuang, K.-J., et al. 2021, NatAs, 5, 197
Ioppolo, S., van Boheemen, Y., Cuppen, H. M., van Dishoeck, E. F., & Linnartz, H. 2011, MNRAS, 413, 2281
Isokoski, K., Bottinelli, S., & Van Dishoeck, E. 2013, A&A, 554, A100
Jiang, G. J., Person, W. B., & Brown, K. G. 1975, JChPh, 62, 1201
Jiménez-Escobar, A., Giuliano, B., Caro, G. M., Cernicharo, J., & Marcelino, N. 2014, ApJ, 788, 19
Jones, B. M., Bennett, C. J., & Kaiser, R. I. 2011, ApJ, 734, 78
Jones, P. A., Burton, M. G., Cunningham, M. R., Tothill, N. F., & Walsh, A. J. 2013, MNRAS, 433, 221
Kahane, C., Ceccarelli, C., Faure, A., & Caux, E. 2013, ApJL, 763, L38
Khoshkhoo, H., & Nixon, E. R. 1973, AcSpA, 29, 603
King, S.-T. 1971, JPhCh, 75, 405
Lacy, J., Baas, F., Allamandola, L., et al. 1984, ApJ, 276, 533
Lee, C.-F., Li, Z.-Y., Ho, P. T., et al. 2017, ApJ, 843, 27
Ligterink, N., Walsh, C., Bhuin, R., et al. 2018, A&A, 612, A88
López-Sepulcre, A., Balucani, N., Ceccarelli, C., et al. 2019, ESC, 3, 2122
López-Sepulcre, A., Jaber, A. A., Mendoza, E., et al. 2015, MNRAS, 449, 2438
Lowenthal, M., Khanna, R., & Moore, M. H. 2002, AcSpA, 58, 73
Lu, H.-C., Chen, H.-K., Cheng, B.-M., Kuo, Y.-P., & Ogilvie, J. F. 2005, JPhB, 38, 3693
Lundell, J., Krajewska, M., & Räsänen, M. 1998, JPCA, 102, 6643
Marcelino, N., Gerin, M., Cernicharo, J., et al. 2018, A&A, 620, A80
Martín-Doménech, R., Öberg, K. I., & Rajappan, M. 2020, ApJ, 894, 98
Mason, N. J., Dawes, A., Holtom, P. D., et al. 2006, FaDi, 133, 311
Meierhenrich, U. J. 2005, Angew. Chem. Int. Ed., 44, 5630
Mendoza, E., Lefloch, B., López-Sepulcre, A., et al. 2014, MNRAS, 445, 151
Meunier, F. C. 2019, J.Catal., 372, 388
Milligan, D. E., & Jacox, M. E. 1964, JChPh, 41, 3032
Milligan, D. E., & Jacox, M. E. 1965, JChPh, 43, 4487
Milligan, D. E., & Jacox, M. E. 1971, JChPh, 54, 927
Muñoz Caro, G. M., Meierhenrich, U. J., Schutte, W. A., et al. 2002, Natur, 416, 403
Neill, J. L., Bergin, E. A., Lis, D. C., et al. 2014, ApJ, 789, 8
Nelander, B. 1980, JChPh, 73, 1026
Noble, J. A., Theule, P., Congiu, E., et al. 2015, A&A, 576, A91
Nuevo, M., Auger, G., Blanot, D., & D'Hendecourt, L. 2008, OLEB, 38, 37
Okabe, H., & Lenzi, M. 1967, JChPh, 47, 5241
Oya, Y., Sakai, N., Watanabe, Y., et al. 2017, ApJ, 837, 174
Potapov, A., Jäger, C., & Henning, T. 2019, ApJ, 880, 12
Prasad, S. S., & Tarafdar, S. P. 1983, ApJ, 267, 603
Qasim, D., Fedoseev, G., Chuang, K.-J., et al. 2020, NatAs, 4, 781
Qasim, D., Lamberts, T., He, J., et al. 2019, A&A, 626, A118
Raunier, S., Chiavassa, T., Duvernay, F., et al. 2004, A&A, 416, 165
Raunier, S., Chiavassa, T., Marinelli, F., Allouche, A., & Aycard, J. 2003, CPL, 368, 594
Rotelli, L., Trigo-Rodríguez, J. M., Moyano-Cambero, C. E., et al. 2016, NatSR, 6, 1
Rubin, R., Swenson, G., Jr., Benson, R., Tigelaar, H., & Flygare, W. 1971, ApJL, 169, L39
Ryazantsev, S. V., Feldman, V. I., & Khriachtchev, L. 2017, JAChS, 139, 9551
Saladino, R., Crestini, C., Ciciriello, F., Costanzo, G., & Di Mauro, E. 2006, OLEB, 36, 523
Schutte, W., & Greenberg, J. 1997, A&A, 317, L43
Schutte, W. A., Allamandola, L. J., & Sandford, S. A. 1993, Sci, 259, 1143
Schutte, W. A., Boogert, A. C. A., Tielens, A. G. G. M., et al. 1999, A&A, 343, 966
Shen, C. J., Greenberg, J. M., Schutte, W. A., & van Dishoeck, E. F. 2004, A&A, 415, 203
Simons, M., Lamberts, T., & Cuppen, H. 2020, A&A, 634, A52
Sivaraman, B., Raja Sekhar, B. N., Nair, B. G., Hatode, V., & Mason, N. J. 2013, AcSpA, 105, 238
Skouteris, D., Vazart, F., Ceccarelli, C., et al. 2017, MNRASL, 468, L1
Song, L., & Kästner, J. 2016, PCCP, 18, 29278
Suhasaria, T., & Mennella, V. 2020, A&A, 641, A88
Suzuki, T., Ohishi, M., Saito, M., et al. 2018, ApJS, 237, 3
Takahiro, Y., Takano, S., Watanabe, Y., et al. 2012, PASJ, 64, 105
Taquet, V., López-Sepulcre, A., Ceccarelli, C., et al. 2015, ApJ, 804, 81
Teles, J. H., Maier, G., Andes Hess, B., et al. 1989, Chemische Berichte, 122, 753
Terwischa van Scheltinga, J., Ligterink, N., Boogert, A., van Dishoeck, E., & Linnartz, H. 2018, A&A, 611, A35
Theule, P., Duvernay, F., Ilmane, A., et al. 2011, A&A, 530, A96
Torrie, B., & Brown, B. 1994, JRSp, 25, 183
van Broekhuizen, F. A., Keane, J. V., & Schutte, W. A. 2004, A&A, 415, 425
Watanabe, N., & Kouchi, A. 2002a, ApJL, 571, L173
Watanabe, N., & Kouchi, A. 2002b, ApJ, 567, 651
Willacy, K., & Millar, T. J. 1998, MNRAS, 298, 562
Yokota, T., & Back, R. 1973, Int. J. Chem. Kinet., 5, 37
Zheng, W., Jewitt, D., Osamura, Y., & Kaiser, R. I. 2008, ApJ, 674, 1242